0026-895X/06/6906-2058–2067$20.00
MOLECULAR PHARMACOLOGY
Copyright © 2006 The American Society for Pharmacology and Experimental Therapeutics
Mol Pharmacol 69:2058–2067, 2006

Vol. 69, No. 6
22665/3117609
Printed in U.S.A.

The Suramin Analog 4,4′,4″,4‴-(Carbonylbis(imino-5,1,3-benzenetriylbis (carbonylimino)))tetra-kis-benzenesulfonic Acid (NF110) Potently Blocks $P2X_3$ Receptors: Subtype Selectivity Is Determined by Location of Sulfonic Acid Groups

Ralf Hausmann, Jürgen Rettinger, Zoltan Gerevich, Sabine Meis, Matthias U. Kassack, Peter Illes, Günter Lambrecht, and Günther Schmalzing

Molecular Pharmacology, RWTH Aachen University, Aachen, Germany (R.H., G.S.); Max-Planck-Institute of Biophysics, Frankfurt am Main, Germany (J.R.); Rudolf-Boehm Institute for Pharmacology and Toxicology, University of Leipzig, Leipzig, Germany (Z.G., P.I.); Department of Pharmaceutical Chemistry, University of Bonn, Bonn, Germany (S.M., M.U.K.); and Department of Pharmacology, University of Frankfurt, Frankfurt am Main, Germany (G.L.)

Received January 17, 2006; accepted March 21, 2006

ABSTRACT

We have previously identified the suramin analog 4,4′,4″,4‴-(carbonylbis(imino-5,1,3-benzenetriylbis(carbonylimino)))tetra-kis-benzene-1,3-disulfonic acid (NF449) as a low nanomolar potency antagonist of recombinant $P2X_1$ receptors. Here, we characterize, by two-electrode voltage-clamp electrophysiology, three isomeric suramin analogs designated *para*-4,4′,4″,4‴-(carbonylbis(imino-5,1,3-benzenetriylbis (carbonylimino)))tetra-kis-benzenesulfonic acid (NF110), *meta*-(3,3′,3″,3‴-(carbonylbis(imino-5,1,3-benzenetriylbis (carbonylimino)))tetra-kis-benzenesulfonic acid (NF448), and *ortho*-(2,2′,2″,2‴-(carbonylbis(imino-5,1,3-benzenetriylbis (carbonylimino)))tetra-kis-benzenesulfonic acid (MK3) with respect to their potency in antagonizing rat P2X receptor-mediated inward currents in *Xenopus laevis* oocytes. *Meta*, *para*, and *ortho* refer to the position of the single sulfonic acid group relative to the amide bond linking the four symmetrically oriented benzenesulfonic acid moieties to the central, invariant suramin core. NF448, NF110, and MK3 were >200-fold less potent in blocking $P2X_1$ receptors than NF449, from which they differ structurally only by having one instead of two sulfonic acid residues per benzene ring. Although the *meta*- and *ortho*-isomers retained $P2X_1$ receptor selectivity, the *para*-isomer NF110 exhibited a significantly increased activity at $P2X_3$ receptors ($K_i \sim 36$ nM) and displayed the following unique selectivity profile among suramin derivatives: $P2X_{2+3} = P2X_3 > P2X_1 > P2X_2 \gg P2X_4 > P2X_7$. The usefulness of NF110 as a $P2X_3$ receptor antagonist in native tissues could be demonstrated by showing that NF110 blocks $\alpha\beta$-methylene-ATP-induced currents in rat dorsal root ganglia neurons with similar potency as recombinant rat $P2X_3$ receptors. Together, these data highlight the importance of both the number and exact location of negatively charged groups for P2X subtype potency and selectivity.

P2X receptors constitute an abundant class of cell surface receptors that open an intrinsic pore that becomes permeable to small cations when exposed to extracellular ATP and related nucleotides (North, 2002). The seven known subunit isoforms, designated $P2X_1$–$P2X_7$, assemble into homotrimeric and heterotrimeric receptor channels (Nicke et al., 1998; Aschrafi et al., 2004; Mio et al., 2005), resulting in large receptor subtype diversity.

Among the numerous sensory processes in which P2X receptors have been implicated, their involvement in nocicep-

This research project is supported by the START-Program of the Faculty of Medicine, RWTH Aachen University (to R.H.); by a grant of the "Fonds der Chemischen Industrie" (to G.L.); and by the Deutsche Forschungsgemeinschaft grants GRK 677/1&2 (to M.U.K.), La 350/7-3 and GRK 137/3 (to G.L.), and Schm 536/6-1; FOR450, TP11 (to G.S.). Preliminary results of this work were presented as a meeting abstract: Hausmann R, Rettinger J, Kassack M, Lambrecht G, and Schmalzing G (2004) Characterization of the novel suramin analog NF110 as a potent $P2X_3$ receptor-selective antagonist. *Naunyn-Schmiedeberg's Arch Pharmacol* **369:**R28.

Article, publication date, and citation information can be found at http://molpharm.aspetjournals.org.

doi:10.1124/mol.106.022665.

ABBREVIATIONS: α,β-meATP, $\alpha\beta$-methylene-adenosine 5′-triphosphate; TNP-ATP, 2′,3′-*O*-(2,4,6-trinitrophenyl)-adenosine 5′-triphosphate; A-317491, 5-([(3-phenoxybenzyl)[(1S)-1,2,3,4-tetrahydro-1-naphthalenyl]amino]carbonyl)-1,2,4-benzenetricarboxylic acid); NF110, 4,4′,4″,4‴-(carbonylbis(imino-5,1,3-benzenetriylbis (carbonylimino)))tetra-kis-benzenesulfonic acid; NF448, 3,3′,3″,3‴-(carbonylbis(imino-5,1,3-benzenetriylbis (carbonylimino)))tetra-kis-benzenesulfonic acid; NF449, 4,4′,4″,4‴-(carbonylbis(imino-5,1,3-benzenetriylbis(carbonylimino)))tetrakis-benzene-1,3-disulfonic acid; MK3, 2,2′,2″,2‴-(carbonylbis(imino-5,1,3-benzenetriylbis (carbonylimino)))tetra-kis-benzenesulfonic acid; NF279, 8,8′-(carbonylbis(imino-4,1-phenylenecarbonylimino-4,1-phenylenecarbonylimino))bis(1,3,5-naphthalenetrisulfonic acid); ORi, sterile oocyte Ringer's; wt, wild-type; DRG, dorsal root ganglia.

tion has attracted particular attention (North, 2004). Pain-sensing sensory neurons of trigeminal, nodose, and dorsal root ganglia express at least six of the seven P2X subunit isoforms (Collo et al., 1996). Interest has been centered on two members, $P2X_2$ and $P2X_3$, which seem to account for the two major types of responses of sensory neurons to ATP or $\alpha\beta$-methylene-ATP (α,β-meATP): 1) a rapidly desensitizing inward current typical for homomeric $P2X_3$ receptors (Rae et al., 1998), and 2) a slowly or nondesensitizing current typical for heteromeric $P2X_{2+3}$ receptors assembled from $P2X_3$ and $P2X_2$ subunits (Lewis et al., 1995). Because $P2X_3$ subunits are almost exclusively confined to sensory neurons, $P2X_3$ subunit-containing receptors represent a promising target for the development of novel analgesic drugs (Chizh and Illes, 2001; Kennedy, 2005; Burnstock, 2006).

Converging evidence for an important role of the $P2X_3$ subunit in nociception comes from gene knockout and pharmacological studies. Sensory neurons of $P2X_3$ knockout mice lacked ATP-inducible desensitizing inward currents and showed reduced pain-related behaviors (Cockayne et al., 2000; Souslova et al., 2000). In addition, post-transcriptional silencing of $P2X_3$ gene expression by intrathecally applied antisense oligonucleotides or short interfering RNA in rodents reduced pain intensity (Barclay et al., 2002; Honore et al., 2002; Dorn et al., 2004). Recently, the nucleotide analog 2′,3′-*O*-(2,4,6-trinitrophenyl)-ATP (TNP-ATP), a high-affinity antagonist of $P2X_1$, $P2X_3$, and $P2X_{2+3}$ receptors (Virginio et al., 1998; Burgard et al., 2000), and A-317491, a high-affinity non-nucleotide antagonist of $P2X_3$ and $P2X_{2+3}$ receptors, have been found to produce antinociceptive effects in various pain models in rodents (Honore et al., 2002; Jarvis et al., 2002; McGaraughty et al., 2003).

Antinociceptive responses were also observed in rodents upon administration of the nonselective P2 antagonist suramin (Driessen et al., 1994; Honore et al., 2002). We have shown the potential of suramin as a lead structure for developing highly potent $P2X_1$ receptor-selective antagonists (Rettinger et al., 2000, 2005; Lambrecht et al., 2002; Horner et al., 2005). Here, we report about the isomeric suramin analogs NF110, NF448, and MK3, which differ from the potent $P2X_1$ receptor-selective antagonist NF449 only in the number (one instead of two) of sulfonic acid groups present in *para*-, *meta*-, or *ortho*-position at each of the four terminal benzene rings (Figs. 1 and 5, A and C). Reducing the number of sulfonic acid groups from eight to four greatly reduced the potency at $P2X_1$ receptors, yet it did not change selectivity per se, because the *meta*- and *ortho*-isomers NF448 and MK3, respectively, still behaved as a distinctly $P2X_1$ receptor selective antagonists. In contrast, the potency of the *para*-isomer, NF110, at $P2X_3$ receptors was greatly enhanced, whereas the potency at $P2X_1$ receptors remained unaffected, resulting in an overall selectivity change in favor of $P2X_3$ receptors. These data demonstrate that both the number and precise position of negatively charged substituents provide a structural basis for altering the selectivity and potency of antagonists at P2X receptor subtypes.

Materials and Methods

Materials. ATP and α,β-meATP were obtained from Sigma-Aldrich (Taufkirchen, Germany). The suramin derivatives NF110, NF448, and MK3 (for chemical structures, see Figs. 1 and 5, A and C) were synthesized as tetrasodium salts (Kassack et al., 2004). Enzymes were obtained from New England Biolabs (Frankfurt, Germany), Epicenter (Madison, WI), Stratagene (La Jolla, CA), or Promega (Heidelberg, Germany). Desoxyoligonucleotides were from QIAGEN GmbH (Hilden, Germany). All other chemicals were purchased from either Sigma-Aldrich or Merck (Darmstadt, Germany).

P2X Receptor Expression in *Xenopus laevis* Oocytes. Plasmids encoding wild-type rat P2X subunits ($rP2X_1$, GenBank accession no. X80477; $rP2X_2$, GenBank accession no. U14414; $rP2X_3$, GenBank accession no. X90651; $rP2X_4$, GenBank accession no. X87763; and $rP2X_7$, GenBank accession no. X95882) and a $rP2X_2$-X_1 chimera comprising the first 47 N-terminal amino acids of the $rP2X_2$ subunit joined in frame with amino acids ^{48}Val-^{399}Ser of the 399-amino acid-long $rP2X_1$ subunit were available from previous studies (Nicke et al., 1998; Aschrafi et al., 2004).

An $rP2X_2$-X_3 chimera was generated by joining, in-frame, the first 47 N-terminal codons of the $rP2X_2$ subunit (^{1}Met-^{47}Tyr) with codons ^{42}Val-^{397}His of the 397-amino acid-long $rP2X_3$ subunit. To this end, SnaB I sites were introduced by site-directed mutagenesis, allowing for blunt-ended cleavage just before corresponding ^{48}Val and ^{42}Val codons of the $rP2X_2$-pNKS2 and $rP2X_3$-pNKS2 plasmids, respectively. The N-terminal $rP2X_2$ sequence was excised with HindIII and SnaBI and ligated in frame between the HindIII site of the vector and the inserted SnaBI cleavage site of $rP2X_3$-pNKS2, thus yielding $rP2X_2$-X_3-pNKS2. The construct was verified by sequencing using an ABI Prism 310 genetic analyzer (Applied Biosystems, Foster City, CA).

Capped cRNAs were synthesized from linearized plasmids and injected at 0.5 $\mu g/\mu l$ in 23- or 50-nl aliquots into follicle cell-free *X. laevis* oocytes using a Nanoliter 2000 injector (WPI, Sarasota, FL). For expression of the heteromeric $rP2X_{2+3}$ combination, a 1:1 (w/w) ratio of $rP2X_2$ and $rP2X_3$ cRNA was injected. Oocytes were maintained at 19°C in sterile oocyte Ringer's (ORi) solution (90 mM NaCl, 1 mM KCl, 1 mM $CaCl_2$, 1 mM $MgCl_2$, and 10 mM HEPES, pH 7.4) supplemented with 50 μg/ml gentamicin.

Two-Electrode Voltage-Clamp Electrophysiology. Agonist-evoked current responses were recorded 1 to 3 days after cRNA injection at ambient temperature (21–24°C) with a conventional two-electrode voltage-clamp (Turbo TEC-05 amplifier; npi Electronics, Tamm, Germany) at a holding potential of −60 mV as described

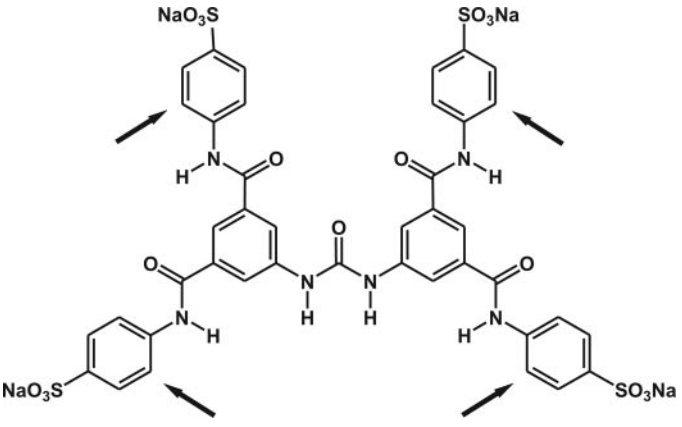

Fig. 1. Chemical structure of NF110. NF110 is designated as a tetravalent suramin derivative, because four aromatic ring systems (benzene rings in the case of NF110) carrying sulfonic acid residues are linked by amide bonds to the central, symmetrically phenyl-substituted urea moiety, which represents the invariant part of suramin. Bivalent suramin analogs such as NF023 and NF279 contain only two amide-bonded aromatic ring systems. Arrows indicate the positions where additional sulfonic acid groups are located on the otherwise structurally identical, previously characterized suramin analog NF449. NF449 blocks $P2X_1$ receptors with subnanomolar potency, but it is a comparatively weak inhibitor of $P2X_3$ receptors (Rettinger et al., 2005). Please note that the sulfonic acid groups of NF110 are in *para*-position relative to the amide bond.

previously (Rettinger et al., 2005). Oocytes were continuously perfused by gravity flow (5–10 ml/min) in a small flow-through chamber (volume ~10 μl) with a nominally calcium-free ORi solution (designated Mg-ORi), in which $CaCl_2$ was replaced by equimolar $MgCl_2$ to avoid a contribution of endogenous Ca^{2+}-dependent Cl^- channels to the ATP response. $rP2X_7$ receptor-dependent currents were recorded in a bathing solution consisting of 94 mM NaCl, 1 mM KCl, 0.1 mM flufenamic acid, and 10 mH HEPES-NaOH, pH 7.4 (Hulsmann et al., 2003).

Dilutions of agonists and antagonists in Mg-ORi were prepared daily and applied by bath perfusion. Switching between bath solutions was controlled by a set of magnetic valves, enabling computer-controlled applications of compounds in a rigorous schedule by using the CellWorks Lite 5.1 software (npi Electronics, Tamm, Germany). For analyzing the antagonist-mediated inhibition of P2X receptor currents, the receptors were activated with agonist concentrations close to the respective EC_{50} value (i.e., 10 μM ATP for $rP2X_2$ and $rP2X_4$ receptors, 1 μM ATP for $rP2X_1$ and $rP2X_3$ receptors) (Rettinger et al., 2000), 10 nM ATP for $P2X_2$-X_1 and $P2X_2$-X_3 chimeras, 100 μM ATP for the $rP2X_7$ receptor, and 1 μM α,β-meATP for the $rP2X_{2+3}$ heteromeric receptor. How agonists and antagonists were applied was dependent on whether desensitizing or nondesensitizing P2X receptors were under study (see below).

Concentration-Inhibition Analysis of Fast Desensitizing P2X Currents. For the analysis of the activation and inhibition of the rapidly desensitizing wt-$rP2X_1$ and wt-$rP2X_3$ receptors, receptors were first repetitively activated in 1- or 2-min intervals with an EC_{50} concentration of ATP until constant current responses were obtained. After this pre-equilibration period and complete ATP washout, oocytes were perfused for 30 s with the desired concentration of antagonist alone, followed by a 5-s-long coapplication of 1 μM ATP and antagonist. Between the applications of incrementally larger concentrations of antagonist, ATP control responses were recorded to monitor rundown or run-up artifacts and to check for complete washout of the antagonist. Thus, each current amplitude (peak current) recorded in the presence of antagonist could be compared for reference with the two flanking control responses to ATP alone. Further details are given in the figure legends.

Concentration-Inhibition Analysis of Nondesensitizing P2X Currents. Oocytes expressing nondesensitizing P2X receptors (defined as a current decrease of <5% over 30 s in the presence of agonist) were superfused with agonist-containing bath solution until a steady-state current was obtained. Then, the superfusion solution was switched to one containing both antagonist and the same concentration of agonist as before. The superfusion was maintained until a steady-state level of inhibition was reached, followed by switching to bath solution alone for drug washout. The percentage of the control response was calculated as the steady-state currents in the absence and presence of antagonist.

Whole-Cell Patch-Clamp Recordings in Dorsal Root Ganglia Neurons. The isolation and culturing of thoracic and lumbar DRGs from 1-day-old male Wistar rats has been described previously (Gerevich et al., 2005). Membrane currents were recorded at a holding a potential of −70 mV by whole-cell configuration patch clamping using an Axopatch 200B amplifier (Axon Instruments). Patch pipettes (3–5 MΩ) were filled with a solution containing 135 mM CsCl, 2 mM $MgCl_2$, 11 mM EGTA, 1 mM $CaCl_2$, 1.5 mM Mg-ATP, and 0.3 mM Li-GTP, and 20 mM HEPES-CsOH, pH 7.3. The external recording solution consisted of 140 mM NaCl, 5 mM KCl, 2 mM $MgCl_2$, 2 mM $CaCl_2$, 11 mM glucose, and 10 mM HEPES-NaOH, pH 7.4. To block the firing of cells during agonist application, 2 mM lidocaine *N*-ethyl bromide was included in the pipette solutions. A pressure-operated, computer-controlled, rapid drug application device (DAD-12; Adams and List, Westbury, NY) was used for drug administration. To induce $P2X_3$ receptor-mediated currents, 10 μM α,β-meATP was applied onto single DRG cells for 1 s in 5-min intervals. The responses to α,β-meATP were constant (Gerevich et al., 2005). After recording of two α,β-meATP-induced currents of approximately the same amplitude (control currents), NF110 was administered in increasing concentrations (0.03–30 μM) to the same cell. For each NF110 concentration, a 5-min preincubation with NF110 was followed by a 1-s test pulse of 10 μM α,β-meATP in the continued presence of NF110 at the same concentration as during preincubation. To estimate the inhibitory effect of NF110, the α,β-meATP-induced current amplitude after the incubation with a certain NF110 concentration was expressed as percentage ± S.E.M. of the control current.

Data Analysis. Data were plotted and fitted using Prism 4 (GraphPad Software Inc., San Diego, CA) and Origin 6.0 (OriginLab Corp., Northampton, MA). Agonist concentration-response curves were produced by measuring the maximal current induced by increasing concentrations of agonist, which were then normalized to the maximal current value obtained with a saturating ATP concentration. Concentration-response curves and half-maximal effective agonist concentrations (EC_{50}) were obtained from curves by iteratively fitting the Hill equation (eq. 1) to the normalized data points pooled from several (n) oocytes:

$$I/I_{max} = 1/(1 + ([EC_{50}/A])^{nH}) \quad (1)$$

where I is the current evoked by agonist concentration A, I_{max} the maximal current response, and n_H the Hill coefficient.

Concentration-inhibition curves and IC_{50} values were derived from nonlinear least-squares fits of eq. 2 to the pooled data points:

$$I_{Ant}/I_{max} = 1/(1 + ([Ant]/IC_{50})^{nH}) \quad (2)$$

where I_{max} is the current response in absence of antagonist (Ant), I_{Ant} is the current response at the respective antagonist concentration, and IC_{50} the antagonist concentration causing 50% inhibition of the current elicited by a given agonist concentration.

Where indicated, IC_{50} values were transformed into inhibition constants (K_i values) by using the classic Cheng-Prusoff equation (Cheng and Prusoff, 1973):

$$K_i = (IC_{50})/(1 + ([ATP]/EC_{50})) \quad (3)$$

which is warranted by the classification of NF110 as a competitive antagonist (see *Results*).

Results are presented as means ± S.E.M. from n experiments. Error bars were omitted in the figures when they were smaller than the symbols used.

Target Specificity of NF110. The pharmacological specificity of NF110 at a fixed concentration of 10 μM was assessed for a total of 33 cell surface receptors, ion channels, transporters, and enzymes by testing in the commercially available diversity profile at Cerep (Celle l'Evescault, France) (http://www.cerep.fr). In addition, the ability of NF110 to block recombinant human $P2Y_1$, $P2Y_2$, and $P2Y_{11}$ receptors was evaluated by Ca^{2+} imaging using Oregon Green 448 as a fluorescent indicator exactly as described previously (Ullmann et al., 2005).

Results

Inhibition of Fast-Desensitizing $rP2X_1$ and $rP2X_3$ Receptor-Mediated Responses by NF110. In functional experiments of native P2X receptors, NF110 was found to antagonize α,β-meATP-induced contractions of the longitudinal smooth muscle of guinea pig ileum more potently than contractions of the rat vas deferens (Kassack et al., 2004). Because this is indicative of a preferential inhibition of (guinea pig) $P2X_3$ over (rat) $P2X_1$ receptors, we have characterized NF110 at rat P2X receptors recombinantly expressed in *X. laevis* oocytes.

For determining concentration-inhibition relationships of NF110 at the fast desensitizing $rP2X_1$ and $rP2X_3$ receptors,

the peak current protocol was used (see *Materials and Methods*). Current traces representative for the application of this protocol to $rP2X_3$ receptor-expressing oocytes are illustrated in Fig. 2A. To assess the time required for the development of the inhibitory effect of NF110, $rP2X_3$ receptor-expressing oocytes were preincubated in pilot experiments for 5 to 60 s with 100 nM NF110 before a test pulse of ATP was applied. Inhibition plateaued after a 15-s preincubation period as shown in Fig. 2B. Therefore, for all subsequent concentration-inhibition measurements, oocytes expressing $rP2X_1$ or $rP2X_3$ receptors were preincubated for exactly 30 s at the desired NF110 concentration and then challenged with 1 μM ATP plus the same NF110 concentration used for preincubation. Fitting the Hill equation to the pooled data yielded IC_{50} values of 201 ± 42 and 90 ± 18 nM for the $rP2X_1$ and $rP2X_3$ receptor, respectively. The corresponding concentration-inhibition curves are included in Fig. 2C.

Antagonist Potencies of NF110 at $rP2X_2$, $rP2X_{2+3}$, $rP2X_4$, and $rP2X_7$ Receptors. The above-mentioned results identified NF110 as the first suramin derivative that is more potent in inhibiting recombinant $rP2X_3$ than $rP2X_1$ receptors. Because the $P2X_3$ subunit exists in vivo not only as homomeric $P2X_3$ receptors but also as functional heteromultimeric assemblies with the $P2X_2$ subunit (designated $P2X_{2+3}$ receptors) (Lewis et al., 1995), the characterization of NF110 was extended to also include these receptor subtypes. $rP2X_{2+3}$ receptors incorporate features of both $P2X_2$ and $P2X_3$ receptors by exhibiting a peculiar nondesensitizing, yet α,β-meATP-sensitive phenotype. Therefore, the protocol for nondesensitizing receptors could be applied for $rP2X_2$ as well as $rP2X_{2+3}$ receptor subtypes. Activation of the homomeric $rP2X_2$ receptor by 10 μM ATP in the presence of increasing concentrations of NF110 yielded an IC_{50} value of 6.2 ± 0.9 μM (Fig. 2C).

Coexpression of $rP2X_2$ and $rP2X_3$ subunits in oocytes results in a mixed population of heterogeneous receptors; these include both the homomeric $rP2X_2$ and $rP2X_3$ receptors as well as the heteromeric $rP2X_{2+3}$ receptors (Liu et al., 2001). To exclude a contribution of homomeric $rP2X_2$ receptors to the current response, 1 μM α,β-meATP was used as an ago-

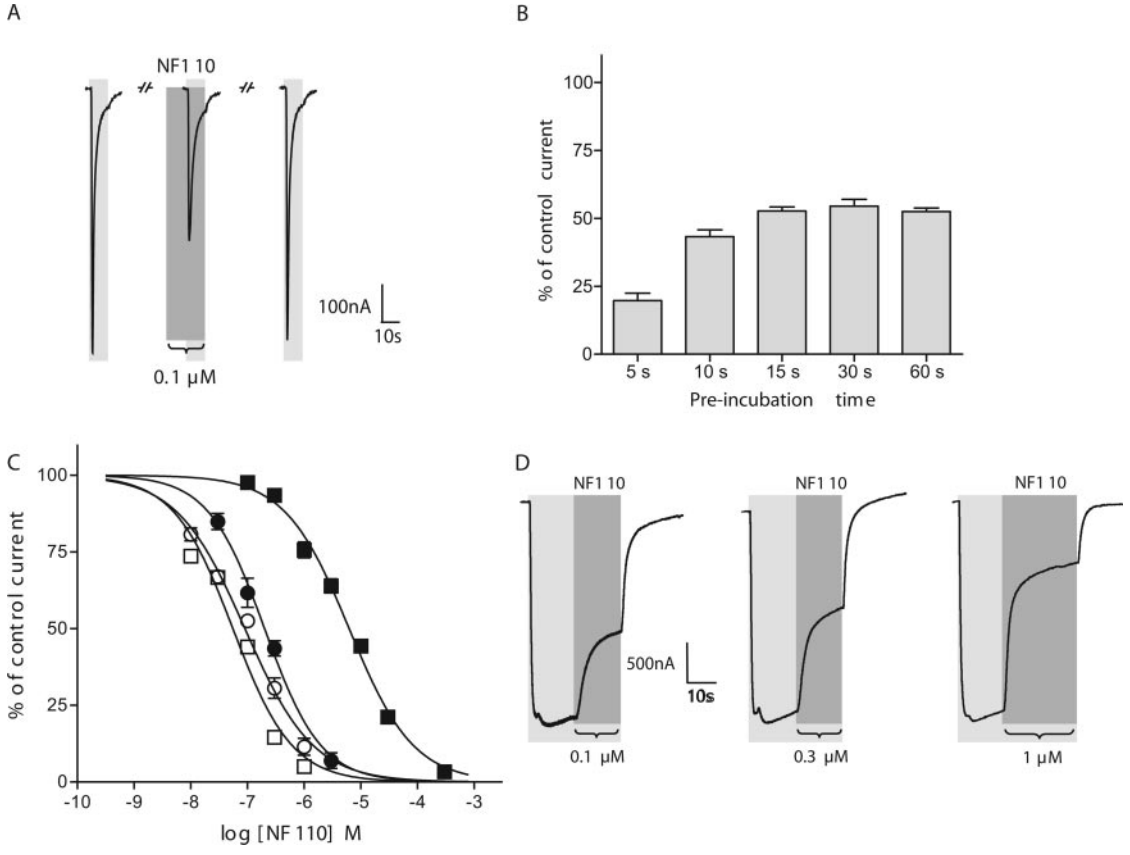

Fig. 2. Antagonist potency of NF110 at $P2X_1$, $P2X_2$, $P2X_{2+3}$, and $P2X_3$ receptors. Light and dark gray areas indicate the duration of application of agonist and NF110, respectively. A, original traces of $rP2X_3$ receptor-mediated currents illustrating the assessment of the inhibitory potency of NF110 from peak current measurements. $rP2X_3$ receptor-expressing oocytes were repetitively activated by 1 μM ATP in 1-min intervals. Between two control measurements, oocytes were pre-equilibrated with the indicated concentration of NF110 for 30 s and then challenged with 1 μM ATP in the continued presence of NF110. The extent of inhibition was judged from the reduction of the peak current amplitude compared with the two flanking control measurements. B, effect of the duration of NF110 preapplication on the inhibition of the fast desensitizing homomeric $rP2X_3$ receptor responses. The bar graph shows the averaged inhibition of current amplitudes elicited by 1 μM ATP after the indicated preincubation times in the presence of 100 nM NF110 as referred to current amplitudes evoked in the absence of NF110 (for details, see A; $n = 5$). C, concentration-inhibition curves. Agonist-induced currents were recorded in the presence of the indicated concentrations of NF110 according to the procedures shown in A and D. ○, $rP2X_3$ homomer; □, $rP2X_{2+3}$ heteromer; ●, $rP2X_1$ homomer; and ■, $rP2X_2$ homomer. In this and all other figures, continuous lines through symbols are fits to the Hill equation. For convenience, all K_i values of NF110 are summarized in Table 1. D, original traces of $rP2X_{2+3}$ receptor-mediated currents illustrating the assessment of the inhibitory potency of NF110 from stationary current measurements. After a stationary current was reached in the presence of 1 μM α,β-meATP, coapplication of NF110 was started (indicated by dark gray area). The current declined until a lower steady state was reached, indicating that inhibition by NF110 was fully developed. Then, application of α,β-meATP and NF110 was terminated. The percentage of the control response was calculated as the ratio of the stationary current in the absence and presence of NF110.

nist, which activates heteromeric $rP2X_{2+3}$ receptors with markedly higher potency than homomeric $rP2X_2$ receptors. Control experiments with oocytes injected solely with cRNA for the $rP2X_2$ subunit showed that >30 μM α,β-meATP was needed to evoke significant inward currents in these cells (results not shown). Original current traces in oocytes coexpressing $rP2X_2$ and $rP2X_3$ subunits are shown in Fig. 2D. α,β-meATP (1 μM) elicited a largely monophasic response consisting of a nondesensitizing current, which in general obscured any rapidly deactivating component attributable to homomeric $rP2X_3$ receptors. Coapplication of NF110 decreased the current amplitude. The extent of current inhibition was quantified as the percentage of current remaining at the end of the NF110-agonist coapplication relative to the current amplitude evoked by agonist alone. Fitting eq. 2 to the pooled data yielded an NF110 IC_{50} value of 55 ± 8.8 nM. The corresponding concentration-inhibition curve is included in Fig. 2C.

Compared with the other rP2X subtypes examined, NF110 was significantly less potent in inhibiting $rP2X_4$ receptors (<45% inhibition at 100 μM NF110; Fig. 3A) and $rP2X_7$ receptors (<5% inhibition at 30 μM NF110; Fig. 3B) irrespective of whether the oocytes were preincubated with NF110 for 15–30 s or not. In regard of the limited availability of NF110, we did not attempt to obtain complete concentration–inhibition curves for these NF110-insensitive receptor subtypes.

Mechanism of $P2X_3$ Receptor Antagonism by NF110. Because $P2X_1$ and $P2X_3$ receptors desensitize rapidly after stimulation with ATP, a binding equilibrium between ATP and a simultaneously applied antagonist cannot be reached during the transient current response (Rettinger et al., 2000). Therefore, the mechanism of inhibition by antagonists cannot be unraveled reliably by the use of nonsteady-state measurements (Burgard et al., 2000; Rettinger et al., 2000; Rettinger and Schmalzing, 2004). In an attempt to overcome this problem, we exploited a nondesensitizing $rP2X_2$-X_3 receptor chimera containing the N-terminal part (amino acids 1–47) of the $rP2X_2$ subunit and the complementary C-terminal part of the $rP2X_3$ subunit (amino acids 42–397). The junction points for joining the N- and C-terminal portions of the $P2X_2$ and $P2X_3$ subunit, Val^{48} and Val^{42}, represent conserved residues in transmembrane domain 1 of both subunits. Because amino acids 1–47 comprise only intracellular portions of the $rP2X_2$ subunit and also because ATP interacts exclusively with the ectodomain (Ennion et al., 2000; Jiang et al., 2000), the ATP binding properties of the chimera can be expected to be identical to that of the wild-type $P2X_3$ receptor. In contrast to the rapidly desensitizing current mediated by the wild-type $rP2X_3$ receptor (Fig. 4A), the $rP2X_2$-X_3 chimera gave rise to stationary, nondesensitizing currents at −60 mV in standard recording solution as long as superfusion with ATP was maintained (Fig. 4B). Concentration-response curves revealed that the $rP2X_2$-X_3 chimera is half-maximally activated by 17.6 ± 1.0 nM ATP or 251 ± 34 nM α,β-meATP (Fig. 4C). These values correspond to an ~40-fold higher ATP potency compared with that of the wild-type $rP2X_3$ receptors (667 ± 143 nM; Fig. 4C). To account for these observations, we assume that elimination of desensitization as realized by the $rP2X_2$-X_3 chimera unmasks nanomolar ATP potency as an inherent feature of the $rP2X_3$ receptor.

Next, we examined whether NF110 inhibits nondesensitizing P2X chimeras with the same potency as that observed for the rapidly desensitizing parental receptors. To this end, we also included a previously characterized nondesensitizing $rP2X_2$-X_1 chimera (Rettinger and Schmalzing, 2004). The chimeras were first activated by superperfusion with ATP at a concentration around their EC_{50} values (10 nM) until a steady-state inward current was achieved in the sustained presence of ATP. Then, the oocytes were superfused with a solution containing the same concentration of ATP plus NF110. As a result of the receptor channel blockade, the current declined until a steady-state level of inhibition was established. To generate concentration-inhibition curves, this procedure was repeated for an ascending series of NF110 concentrations, followed by washout of NF110 and ATP. The extent of NF110-induced inhibition of the $rP2X_2$-X_1 and $rP2X_2$-X_3 chimeras was quantified as the percentage of stationary current remaining in the presence of NF110 relative to the stationary current amplitude elicited by ATP in the absence of NF110. A fit of the Hill equation to the pooled data yielded IC_{50} values for NF110 of 124 ± 32 and 55 ± 12.3 nM at the $rP2X_2$-X_1 and $rP2X_2$-X_3 receptor chimera, respectively (Fig. 4D). Together, these data indicate that NF110 inhibits $rP2X_2$-X_1 and $rP2X_2$-X_3 chimeras with similar potencies as the corresponding wild-type $rP2X_1$ and $rP2X_3$ receptors, respectively.

Next, ATP concentration-response curves were generated in the absence and presence of NF110 at the $rP2X_2$-X_3 chimera. Increasing NF110 concentration produced a parallel rightward shift of the ATP concentration-response curve without changing the maximal response (Fig. 4E). Schild analysis (Fig. 4E, inset) yielded a regression slope of 1.14 ± 0.15, which is not significantly different from unity. On con-

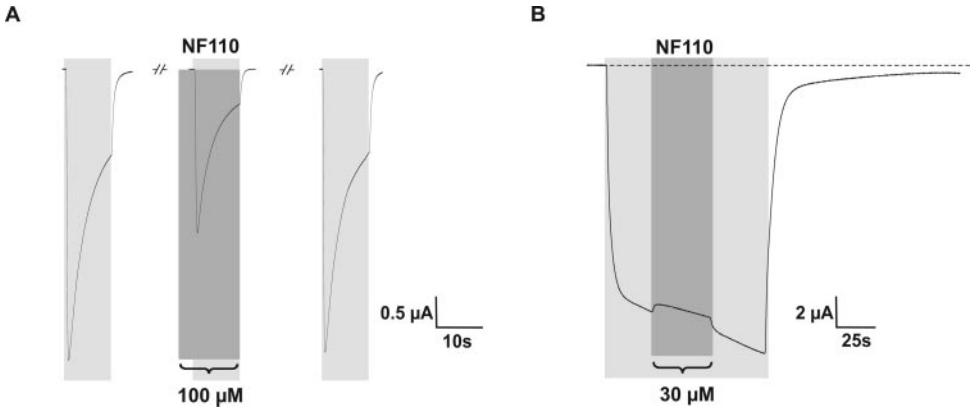

Fig. 3. Antagonist potency of NF110 at $P2X_4$ and $P2X_7$ receptors. Light and dark gray areas indicate the duration of application of agonist and NF110, respectively. A, inhibition by NF110 of inward currents elicited by 10 μM ATP from $rP2X_4$ receptor-expressing oocytes was assessed by applying the peak current protocol. B, typical current trace from $rP2X_7$ receptor-expressing oocytes challenged with 100 μM free ATP. Application of 30 μM NF110 in the continued presence of ATP resulted in a slight reduction of the linearly increasing current component and a slight increase to initial values, when the NF110 application was discontinued.

straining the slope to unity, a pA_2 value of 7.0 was obtained. Together, these data are strongly supportive of a competitive antagonism of NF110 on $P2X_3$ receptors.

Effect of the Positional NF110 Isomers NF448 and MK3, on $P2X_1$, $P2X_2$, and $P2X_3$ Receptor-Mediated Currents. The structure of NF110 differs from that of the $P2X_1$-selective antagonist NF449 solely by the presence of only four (instead of eight) sulfonic acid groups, highlighting the importance of negatively charged groups in P2X subtype selectivity. To examine the importance of the position of the sulfonic acid groups for P2X receptor subtype selectivity, the positional NF110 isomers NF448 and MK3 were exploited. Although NF448 and MK3 differ from NF110 solely by carrying the four sulfonic acid groups in *meta*- or *ortho*- instead of *para*-position (Fig. 5, A and C), respectively, their selectivity profiles were markedly different: NF448 and MK3 most potently inhibited $rP2X_1$ receptor-mediated currents, displaying IC_{50} values of 181 ± 45 nM (n = 6) and 65 ± 14 nM (n = 5), respectively. Inhibition of $P2X_2$ or $P2X_3$ receptor-mediated currents occurred only at significantly higher concentrations of NF448 and MK3 (Fig. 5, B and D). Thus, the exact position of the sulfonic acid groups is of crucial importance for P2X subtype selectivity of these suramin derivatives.

Potency of NF110 at Endogenous P2X Receptors in Rat DRG Neurons. To examine whether NF110 is capable of inhibiting native $P2X_3$ receptors of nociceptive neurons from the rat with similar potency as oocyte-expressed recombinant $rP2X_3$ receptors, DRG neurons of 1-day-old rats were used. $P2X_3$ receptors are found selectively in a subpopulation of DRG neurons and are thought to contribute to the processing of pain information. α,β-meATP applied in a submaxi-

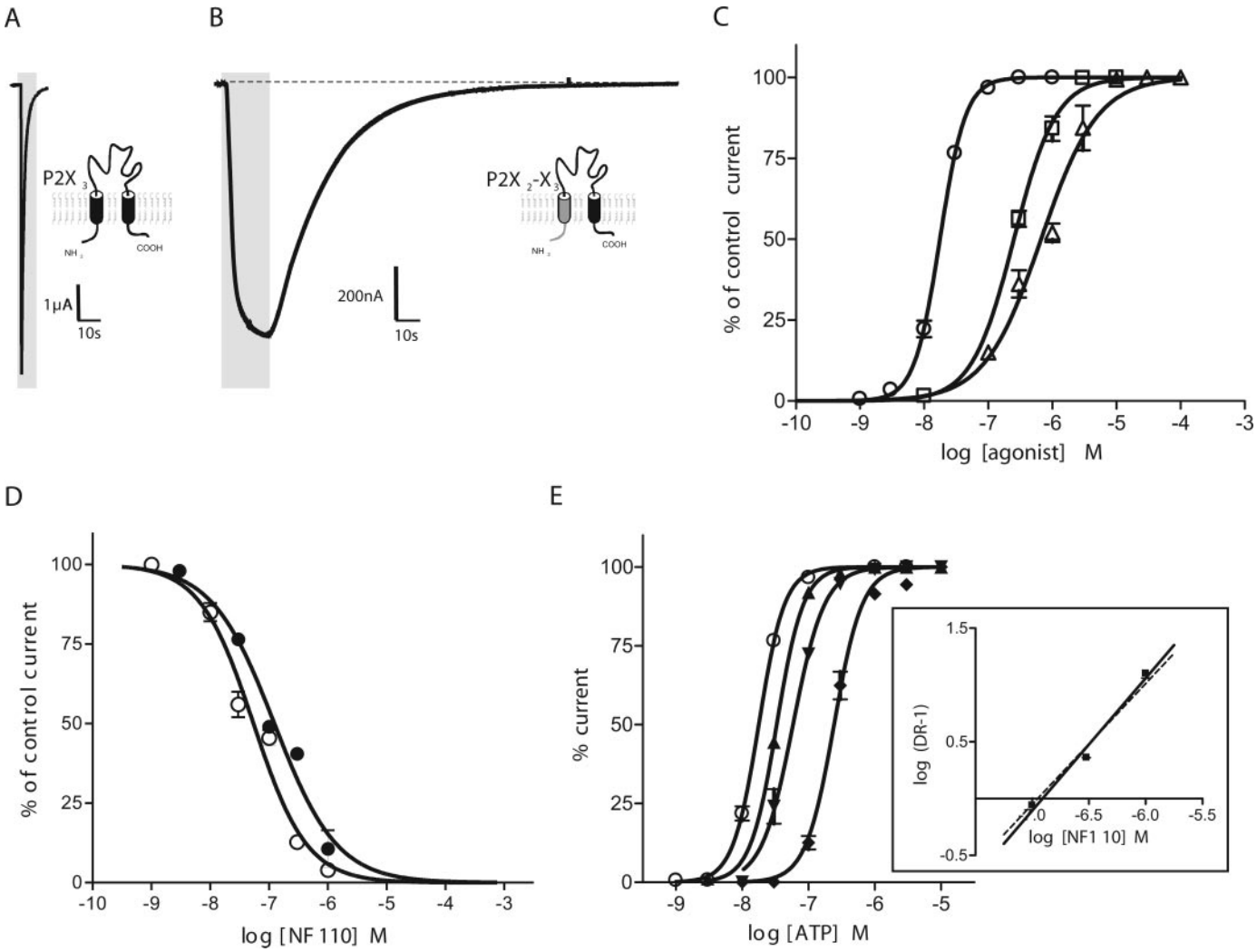

Fig. 4. Assessing the mechanism of NF110-induced inhibition of $rP2X_3$ receptors by exploiting a nondesensitizing $rP2X_2$-X_3 chimera. A and B, traces elicited by 10 μM ATP (denoted by gray areas) in oocytes expressing the wild-type $rP2X_3$ receptor or the $rP2X_2$-X_3 chimera. Note that the chimera deactivated very slowly upon ATP washout. Schematics illustrate the membrane topology of P2X receptors and the swapped domains originating from the $rP2X_2$ subunit (gray) and the $rP2X_3$ subunit (black). C, agonist concentration-response curves for the $rP2X_2$-X_3 chimera (○, ATP: EC_{50} = 17.6 ± 1.0 nM and n_H = 2.2 ± 0.1, n = 7; □, α,β-meATP: EC_{50} = 251 ± 34 nM and n_H = 1.3 ± 0.1, n = 7) and the $rP2X_3$ receptor (△, ATP: EC_{50} = 667 ± 143 nM and n_H = 1.0 ± 0.1, n = 7). Currents were normalized to those elicited by saturating agonist concentrations. D, concentration-inhibition curves. Agonist-induced stationary currents were recorded in the presence of the indicated concentrations of NF110 according to the protocol shown in Fig. 2D. ○, $rP2X_2$-X_3 chimera; ●, $rP2X_2$-X_1 chimera. E, NF110 is a competitive antagonist at the $rP2X_2$-X_3 chimera. ATP concentration–response curves for the $rP2X_2$-X_3 chimera in the absence (○) and presence of NF110 (▲, 100 nM; ▼, 300 nM; and ♦, 1000 nM). Inset, Schild plot derived from this data set. The solid line is a linear regression with a slope of 1.14 ± 0.15 (not significantly different from unity; $p > 0.05$). Constraining the slope to unity (dashed line) yielded a pA_2 value of 7.0.

mally effective concentration of 10 μM every 5 min onto cultured small-diameter (20- to 35-μm) DRG neurons evoked rapidly desensitizing currents with a peak amplitude of 675 ± 106 pA (n = 16). Sensitivity to α,β-meATP and fast desensitization identifies these currents as $P2X_3$ receptor-mediated (Rae et al., 1998). NF110 concentration-dependently inhibited the α,β-meATP-evoked currents with an IC_{50} value of 527 ± 304 nM (n = 5–12) (Fig. 6). A K_i value of 48 nM was calculated using the Cheng-Prusoff equation and an EC_{50} value for α,β-meATP of 1 μM at $P2X_3$ receptors (Khakh et al., 2001).

Activity of NF110 toward a Panel of Drug Targets, Including P2Y Receptors. NF110 was assessed by a commercial profiling service (Cerep) for its interference with a total of 33 non-P2X receptor drug target molecules. NF110 was considered inactive (IC_{50} > 10 μM) toward all targets tested. NF110 was also inactive (IC_{50} > 10 μM) toward $P2Y_1$, $P2Y_2$, and $P2Y_{11}$ receptors stably expressed in astrocytoma cells.

Discussion

Selectivity Profile of NF110 versus Other P2X Receptor Antagonists. We have shown by two-electrode voltage-clamp electrophysiology that the tetravalent suramin analog NF110 (Fig. 1) inhibits P2X receptor subtypes recombinantly expressed in *X. laevis* oocytes; these receptors can be ranked by their potencies, based on K_i values (Table 1): $rP2X_{2+3}$ = $rP2X_3$ > $rP2X_1$ > $rP2X_2$ ≫ $rP2X_4$ > $rP2X_7$. Homomeric $rP2X_3$ receptors are blocked by NF110 with virtually the same potency as heteromeric $rP2X_{2+3}$ receptors. The $P2X_3$ selectivity of NF110 over $P2X_1$ receptors (2-fold) is lower than that of the Abbott compound A-317491 (115-fold) (Jarvis et al., 2002) and more reminiscent to that of TNP-ATP, which also blocks $P2X_1$, $P2X_3$, and $P2X_{2+3}$ receptors with similar potency close to 1 nM (Virginio et al., 1998).

Suramin Derivatives Are Competitive Inhibitors of P2X Receptors. We have previously shown for the desensitizing $rP2X_1$ receptor that the $P2X_1$ receptor-selective

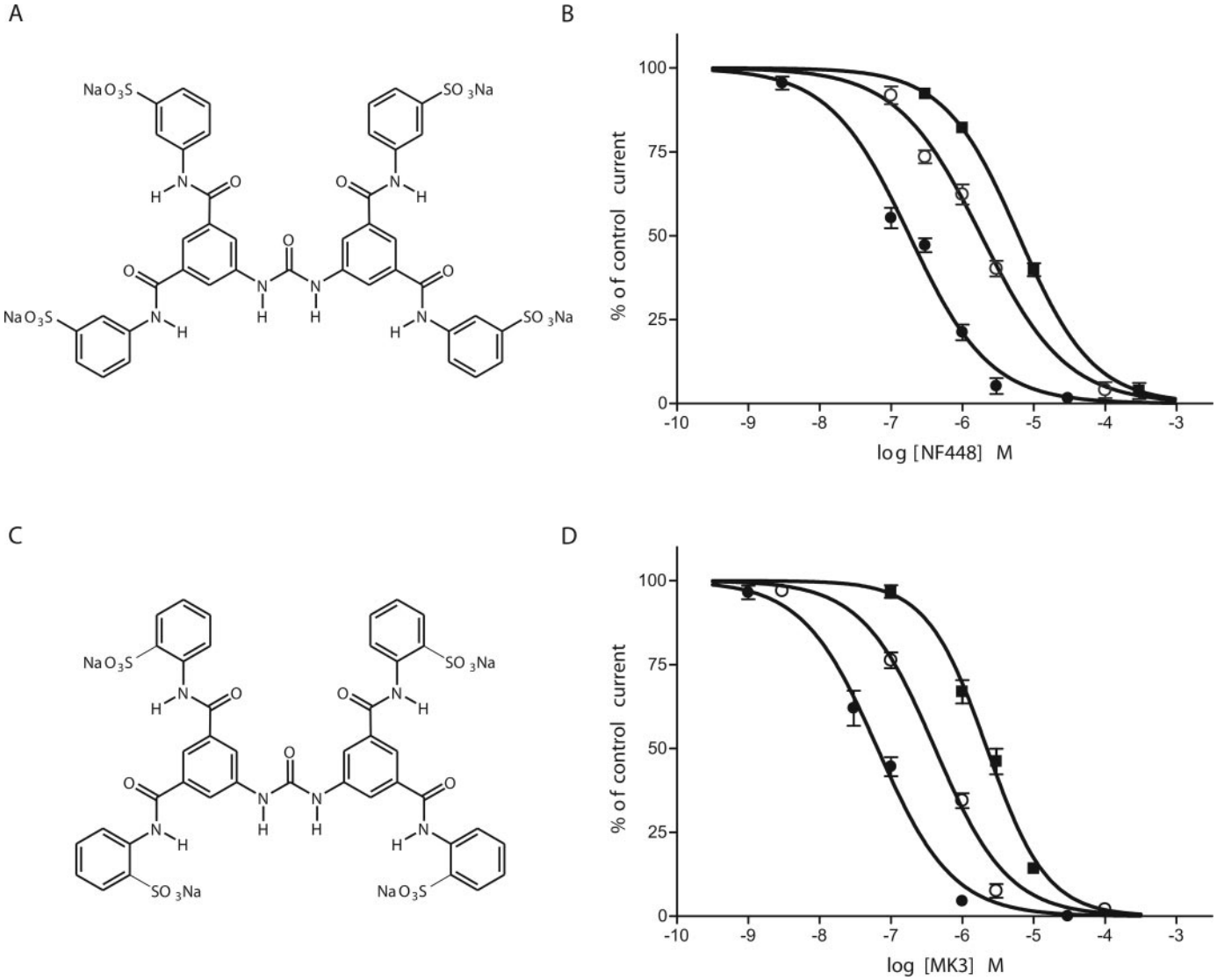

Fig. 5. Antagonist potency of NF448 and MK3 at $P2X_1$, $P2X_2$, and $P2X_3$ receptors. A and C, chemical structures of NF448 and MK3, which contain the sulfonic acid groups in *meta*- and *ortho*-position, respectively, in contrast to the *para*-isomer NF110 (Fig. 1). B, concentration-inhibition curves of NF448 at wild-type $rP2X_1$, $rP2X_2$, and $rP2X_3$ receptors. ●, $rP2X_1$ homomer; ■, $rP2X_2$ homomer; and ○, $rP2X_3$ homomer. D, concentration-inhibition curves of MK3 at wild-type $rP2X_1$, $rP2X_2$, and $rP2X_3$ receptors. ●, $rP2X_1$ homomer; ■, $rP2X_2$ homomer; and ○, $rP2X_3$ homomer.

suramin derivative NF279 causes not only a rightward shift of the ATP concentration-response curves but also a depression of the maximal current response to ATP, when oocytes are pre-equilibrated with high concentrations of NF279 (Rettinger et al., 2000). Although insurmountable antagonism may be indicative of noncompetitive antagonism, a similar inhibitory pattern, called a hemi-equilibrium, can also occur if a short-acting agonist is combined with a slowly dissociating competitive antagonist. In terms of fast-desensitizing P2X receptors, the short duration of the current transient leaves little time for a slowly unbinding antagonist to equilibrate with the fast binding of ATP. The rapidly binding but slowly unbinding TNP-ATP represents a pertinent example of this problem. Based on maximum current depression, TNP-ATP was first interpreted to be a noncompetitive antagonist of the fast-desensitizing recombinant $rP2X_3$ receptor (Virginio et al., 1998). However, re-examination at nondesensitizing $rP2X_{2+3}$ receptors revealed a competitive mechanism of inhibition for TNP-ATP (Burgard et al., 2000) that also applies to homomeric $rP2X_3$ receptors (Neelands et al., 2003).

To resolve the mechanism of antagonism by NF110, without the bias imposed by rapid desensitization, we exploited the nondesensitizing $rP2X_2$-X_3 chimera that allowed us to determine current inhibition under favorable steady-state conditions. In this construct, desensitization is virtually fully eliminated by substitution of the cytoplasmic N-terminal tail and the first membrane domain corresponding to the first 41 amino acids of the $P2X_3$ subunit, respectively, with a complementary part of the $rP2X_2$ subunit. The pivotal feature of this chimera as a surrogate for the wild-type $P2X_3$ receptor is that the comparably small $rP2X_2$ portion is not extracellularly accessible. Therefore, the binding properties of the $rP2X_2$-X_3 chimera described here and the previously published $rP2X_2$-X_1 chimera (Werner et al., 1996; Rettinger and Schmalzing, 2004; Rettinger et al., 2005), at least for polar ligands, are determined by the receptor subunit providing the ectodomain. This view is strongly supported by several observations: 1) like the wild-type $P2X_3$ receptor, the $rP2X_2$-X_3 chimera was activated with high potency by α,β-meATP, which is a low potency agonist for $rP2X_2$ receptors; 2) the suramin analog NF110 blocked the chimera and the corresponding wild-type $rP2X_3$ receptor with virtually the same IC_{50} value, whereas more than 100-fold higher NF110 concentrations were required for blocking the $rP2X_2$ receptor. Essentially the same conclusions were reached in a study, in which similar nondesensitizing human chimeric P2X receptor constructs were used for assessing the antagonistic mechanisms of A-317491 and TNP-ATP (Neelands et al., 2003).

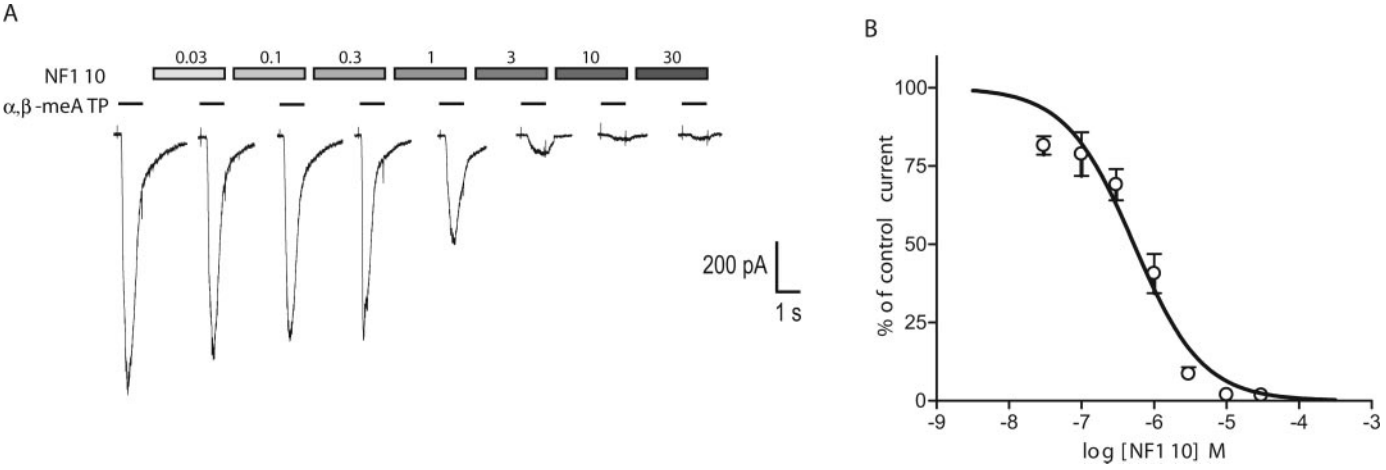

Fig. 6. Antagonist potency of NF110 at endogenous $P2X_3$ receptors in DRG neurons. A, patch-clamp recordings from a neuron that was activated for 1 s in 5-min intervals with 10 μM α,β-meATP (thin bars) in the absence and presence of ascending NF110 concentrations (gray rectangles). B, NF110 concentration-inhibition curve. Data points are based on peak current measurements as outlined in A. IC_{50} = 527 ± 304 nM and n_H = 0.92 ± 0.16; $n \geq 5$.

TABLE 1

Potencies of suramin analogs at recombinant P2X receptors

The Cheng-Prusoff equation (eq. 3) was used to calculate K_i values from the IC_{50} values determined in this study for NF110, NF448, MK3 (Figs. 2, 4, and 5) and the published IC_{50} values for NF449 (Rettinger et al., 2005). Also used in the calculation were the following EC_{50} values obtained for the various P2X receptor subtypes in this laboratory: 0.68 μM ATP ($rP2X_1$), 19.9 μM ATP ($rP2X_2$), 0.67 μM ATP ($rP2X_3$), 17.6 μM ATP ($rP2X_2$-X_3), and 1.7 μM α,β-meATP ($rP2X_{2+3}$). A competitive antagonism is supported by a Schild plot analysis (Fig. 4E). *n* indicates the number of independent experiments.

Receptor	NF110 (*para*-SO_3^-)			NF448 (*meta*-SO_3^-)			MK3 (*ortho*-SO_3^-)			NF449 (*para-*, *ortho*-SO_3^-)	
	K_i	Normalized K_i[a]	*n*	K_i	Normalized K_i[b]	*n*	K_i	Normalized K_i[c]	*n*	K_i	Normalized K_i[d]
	nM			*nM*			*nM*			*nM*	
$rP2X_1$	82 ± 17	2.3	5	74 ± 18	1	5	26 ± 6	1	5	0.11 ± 0.01	1
$rP2X_2$	4144 ± 613	115	6	4070 ± 526	55	4	1469 ± 247	57	5	~19,024	>250,000
$rP2X_3$	36 ± 7	1	6	733 ± 164	10	6	166 ± 29	6	6	737 ± 81	6609
$rP2X_2$-X_3	35 ± 8	1	5	N.D.			N.D.			N.D.	
$rP2X_{2+3}$	35 ± 7	1	6	N.D.			N.D.			76 ± 6	691

N.D., not determined.
[a] Normalized to K_i value of NF110 of 36 nM for the $rP2X_3$ receptor.
[b] Normalized to K_i value of NF448 of 74 nM for the $rP2X_1$ receptor.
[c] Normalized to K_i value of MK3 of 26 nM for the $rP2X_1$ receptor.
[d] Normalized to K_i value of NF449 of 0.11 nM for the $rP2X_1$ receptor.

The data obtained with our rP2X$_2$-X$_3$ chimeric receptors indicate that NF110 meets the criteria for a competitive antagonist. First, increasing NF110 concentrations produced a parallel rightward shift of the ATP concentration-response curve without changing the maximal response. Second, Schild analysis yielded a slope close to unity. The pA_2 value of 7.0 for the P2X$_2$-X$_3$ chimera is in reasonable agreement with the estimated K_i value of 36 nM (pK_i = 7.4) at wild-type P2X$_3$ receptors (Table 1). A competitive mechanism of inhibition by suramin analogs is consistent with previous findings showing that the bivalent suramin analog NF279 acts as a competitive blocker of a nondesensitizing rP2X$_2$-X$_1$ chimera (Rettinger and Schmalzing, 2004).

Rat P2X$_3$ and P2X$_1$ Receptors Share Nanomolar ATP Potency That Is Masked by Desensitization. Strikingly, both the rP2X$_2$-X$_1$ and the rP2X$_2$-X$_3$ chimera are half-maximally activated by 200- or 40-fold lower ATP concentrations than the wild-type rP2X$_1$ and rP2X$_3$ receptors, respectively. Nanomolar potency for ATP is also a feature of the wild-type rP2X$_1$ receptor, but it is obscured by desensitization (Rettinger and Schmalzing, 2004). The micromolar ATP potency deduced under nonsteady-state conditions from peak current measurements represents no more than an amalgam of activation and desensitization. Present data indicate that the rP2X$_3$ receptor (EC_{50} ~ 17 nM) shares nanomolar ATP potency with the rP2X$_1$ receptor (EC_{50} ~ 3 nM) (Rettinger and Schmalzing, 2004). This is not only apparent from the concentration-response curves at the two chimeras but also from the extremely slow current deactivation after agonist washout (Fig. 4B), reflecting slow agonist unbinding (Rettinger and Schmalzing, 2004). The remarkable ATP sensitivity of rP2X$_3$ receptors has already been noted in previous experiments (He et al., 2002). Interestingly, human counterparts of these chimeras lack this high ATP sensitivity and deactivate rapidly after agonist washout (Neelands et al., 2003). Sequence variations between human and rat P2X$_3$ receptors are likely to account for this phenomenon.

The Role of Sulfonic Acid Groups for P2X Receptor Subtype Selectivity and Potency. Using suramin as a lead, we have previously shown that the potency for the P2X$_1$ receptor, in particular, can be increased tremendously by appropriate structural modifications. The most potent P2X$_1$ receptor-selective antagonist identified so far, the tetravalent suramin derivative NF449, exhibits IC_{50} values of 0.05 and 0.3 nM at recombinant human and rat P2X$_1$ receptors, respectively; NF449 is thus >3000-fold more potent than the bivalent parent compound suramin (Lambrecht et al., 2002; Hulsmann et al., 2003; Rettinger et al., 2005). In contrast, ~6000-fold higher NF449 concentrations were needed to block rP2X$_3$ receptors (Rettinger et al., 2005). To allow a direct comparison with NF110, K_i values of NF449 at recombinant rP2X$_1$, rP2X$_2$, and rP2X$_3$ receptors were calculated from published IC_{50} values and included in Table 1.

Sulfonic acid groups influence the antagonistic properties of the suramin derivatives in two aspects. 1) Comparison of the structure and antagonistic potency of NF449 with NF110, NF448, or MK3 reveals that a higher number of sulfonic acid groups has a favorable effect on the potency to block P2X$_1$ receptors. Structurally, NF110 and its isomers differ from NF449 solely by containing only four instead of eight sulfonic acid residues (Figs. 1 and 5), yet these compounds are >200-fold less potent than NF449 in inhibiting the rat P2X$_1$ receptor. A larger number of possible electrostatic interactions of NF449 may account for this effect. Mutagenesis studies implicate that conserved positively charged amino acids close to the external entry of the channel pore (K68, R292, and K309 of the rP2X$_1$ receptor) contribute to ATP binding by attracting the negative charges of the phosphate groups (Ennion et al., 2000; Jiang et al., 2000; Egan et al., 2004). It is likely that these and other positively charged residues play also a role in the binding of the suramin derivatives (Jacobson et al., 2004). 2) The exact position of the sulfonic acid groups seems to be of crucial importance for P2X subtype selectivity. Changing the position of the single sulfonic acid group from *ortho* or *meta* to *para* as realized in NF110 led to a marked increase in P2X$_3$ receptor potency without grossly affecting P2X$_1$ receptor potency.

The observed competitive antagonism combined with the crucial role of negatively charged groups in achieving high potency interactions suggest that the extracellular ATP binding pocket on P2X receptors accommodates at least part of the suramin molecule. At least some of the sulfonic acid groups seem to interact electrostatically with the basic amino acids that are physiologically involved in attracting the phosphate groups of ATP. Together, the present study re-emphasizes the value of suramin as a lead compound for the development of P2X receptor subtype-selective antagonists. The observation that the number and the position of sulfonic acid groups profoundly influence subtype selectivity may be helpful for structural optimization of drugs targeting P2X receptors.

Acknowledgments

We thank Ursula Braam for expert technical assistance in molecular biology experiments.

References

Aschrafi A, Sadtler S, Niculescu C, Rettinger J, and Schmalzing G (2004) Trimeric architecture of homomeric P2X$_2$ and heteromeric P2X$_{1+2}$ receptor subtypes. *J Mol Biol* **342:**333–343.

Barclay J, Patel S, Dorn G, Wotherspoon G, Moffatt S, Eunson L, Abdel'al S, Natt F, Hall J, Winter J, et al. (2002) Functional downregulation of P2X$_3$ receptor subunit in rat sensory neurons reveals a significant role in chronic neuropathic and inflammatory pain. *J Neurosci* **22:**8139–8147.

Burgard EC, Niforatos W, van Biesen T, Lynch KJ, Kage KL, Touma E, Kowaluk EA, and Jarvis MF (2000) Competitive antagonism of recombinant P2X$_{2/3}$ receptors by 2′,3′-*O*-(2,4,6-trinitrophenyl) adenosine 5′-triphosphate (TNP-ATP). *Mol Pharmacol* **58:**1502–1510.

Burnstock G (2006) Purinergic P2 receptors as targets for novel analgesics. *Pharmacol Ther*, in press.

Cheng Y and Prusoff WH (1973) Relationship between the inhibition constant (K_i) and the concentration of inhibitor which causes 50 per cent inhibition (I_{50}) of an enzymatic reaction. *Biochem Pharmacol* **22:**3099–3108.

Chizh BA and Illes P (2001) P2X receptors and nociception. *Pharmacol Rev* **53:**553–568.

Cockayne DA, Hamilton SG, Zhu QM, Dunn PM, Zhong Y, Novakovic S, Malmberg AB, Cain G, Berson A, Kassotakis L, et al. (2000) Urinary bladder hyporeflexia and reduced pain-related behaviour in P2X$_3$-deficient mice. *Nature (Lond)* **407:**1011–1015.

Collo G, North RA, Kawashima E, Merlo-Pich E, Neidhart S, Surprenant A, and Buell G (1996) Cloning of P2X$_5$ and P2X$_6$ receptors and the distribution and properties of an extended family of ATP-gated ion channels. *J Neurosci* **16:**2495–2507.

Dorn G, Patel S, Wotherspoon G, Hemmings-Mieszczak M, Barclay J, Natt FJ, Martin P, Bevan S, Fox A, Ganju P, et al. (2004) siRNA relieves chronic neuropathic pain. *Nucleic Acids Res* **32:**e49.

Driessen B, Reimann W, Selve N, Friderichs E, and Bültmann R (1994) Antinociceptive effect of intrathecally administered P2 purinoceptor antagonists in rats. *Brain Res* **666:**182–188.

Egan TM, Cox JA, and Voigt MM (2004) Molecular structure of P2X receptors. *Curr Top Med Chem* **4:**821–829.

Ennion S, Hagan S, and Evans RJ (2000) The role of positively charged amino acids in ATP recognition by human P2X$_1$ receptors. *J Biol Chem* **275:**29361–29367.

Gerevich Z, Muller C, and Illes P (2005) Metabotropic P2Y(1) receptors inhibit P2X(3) receptor-channels in rat dorsal root ganglion neurons. *Eur J Pharmacol* **521:**34–38.

He ML, Koshimizu TA, Tomic M, and Stojilkovic SS (2002) Purinergic $P2X_2$ receptor desensitization depends on coupling between ectodomain and C-terminal domain. *Mol Pharmacol* **62:**1187–1197.
Honore P, Mikusa J, Bianchi B, McDonald H, Cartmell J, Faltynek C, and Jarvis MF (2002) TNP-ATP, a potent $P2X_3$ receptor antagonist, blocks acetic acid-induced abdominal constriction in mice: comparison with reference analgesics. *Pain* **96:** 99–105.
Horner S, Menke K, Hildebrandt C, Kassack MU, Nickel P, Ullmann H, Mahaut-Smith MP, and Lambrecht G (2005) The novel suramin analogue NF864 selectively blocks $P2X_1$ receptors in human platelets with potency in the low nanomolar range. *Naunyn-Schmiedeberg's Arch Pharmacol* **372:**1–13.
Hulsmann M, Nickel P, Kassack M, Schmalzing G, Lambrecht G, and Markwardt F (2003) NF449, a novel picomolar potency antagonist at human $P2X_1$ receptors. *Eur J Pharmacol* **470:**1–7.
Jacobson KA, Costanzi S, Ohno M, Joshi BV, Besada P, Xu B, and Tchilibon S (2004) Molecular recognition at purine and pyrimidine nucleotide (P2) receptors. *Curr Top Med Chem* **4:**805–819.
Jarvis MF, Burgard EC, McGaraughty S, Honore P, Lynch K, Brennan TJ, Subieta A, van Biesen T, Cartmell J, Bianchi B, et al. (2002) A-317491, a novel potent and selective non-nucleotide antagonist of $P2X_3$ and $P2X_{2/3}$ receptors, reduces chronic inflammatory and neuropathic pain in the rat. *Proc Natl Acad Sci USA* **99:**17179–17184.
Jiang LH, Rassendren F, Surprenant A, and North RA (2000) Identification of amino acid residues contributing to the ATP-binding site of a purinergic P2X receptor. *J Biol Chem* **275:**34190–34196.
Kassack MU, Braun K, Ganso M, Ullmann H, Nickel P, Boing B, Muller G, and Lambrecht G (2004) Structure-activity relationships of analogues of NF449 confirm NF449 as the most potent and selective known $P2X_1$ receptor antagonist. *Eur J Med Chem* **39:**345–357.
Kennedy C (2005) P2X receptors: targets for novel analgesics? *Neuroscientist* **11:** 345–356.
Khakh BS, Burnstock G, Kennedy C, King BF, North RA, Seguela P, Voigt M, and Humphrey PP (2001) International union of pharmacology. XXIV. Current status of the nomenclature and properties of P2X receptors and their subunits. *Pharmacol Rev* **53:**107–118.
Lambrecht G, Braun K, Damer M, Ganso M, Hildebrandt C, Ullmann H, Kassack MU, and Nickel P (2002) Structure-activity relationships of suramin and pyridoxal-5′-phosphate derivatives as P2 receptor antagonists. *Curr Pharm Des* **8:**2371–2399.
Lewis C, Neidhart S, Holy C, North RA, Buell G, and Surprenant A (1995) Coexpression of $P2X_2$ and $P2X_3$ receptor subunits can account for ATP-gated currents in sensory neurons. *Nature (Lond)* **377:**432–435.
Liu M, King BF, Dunn PM, Rong W, Townsend-Nicholson A, and Burnstock G (2001) Coexpression of $P2X_3$ and $P2X_2$ receptor subunits in varying amounts generates heterogeneous populations of P2X receptors that evoke a spectrum of agonist responses comparable with that seen in sensory neurons. *J Pharmacol Exp Ther* **296:**1043–1050.
McGaraughty S, Wismer CT, Zhu CZ, Mikusa J, Honore P, Chu KL, Lee CH, Faltynek CR, and Jarvis MF (2003) Effects of A-317491, a novel and selective $P2X_3$/$P2X_{2/3}$ receptor antagonist, on neuropathic, inflammatory and chemogenic nociception following intrathecal and intraplantar administration. *Br J Pharmacol* **140:**1381–1388.
Mio K, Kubo Y, Ogura T, Yamamoto T, and Sato C (2005) Visualization of the trimeric $P2X_2$ receptor with a crown-capped extracellular domain. *Biochem Biophys Res Commun* **337:**998–1005.
Neelands TR, Burgard EC, Uchic ME, McDonald HA, Niforatos W, Faltynek CR, Lynch KJ, and Jarvis MF (2003) 2′, 3′-*O*-(2,4,6,Trinitrophenyl)-ATP and A-317491 are competitive antagonists at a slowly desensitizing chimeric human $P2X_3$ receptor. *Br J Pharmacol* **140:**202–210.
Nicke A, Bäumert HG, Rettinger J, Eichele A, Lambrecht G, Mutschler E, and Schmalzing G (1998) $P2X_1$ and $P2X_3$ receptors form stable trimers: a novel structural motif of ligand-gated ion channels. *EMBO (Eur Mol Biol Organ) J* **17:**3016–3028.
North RA (2002) Molecular physiology of P2X receptors. *Physiol Rev* **82:**1013–1067.
North RA (2004) $P2X_3$ receptors and peripheral pain mechanisms. *J Physiol (Lond)* **554:**301–308.
Rae MG, Rowan EG, and Kennedy C (1998) Pharmacological properties of $P2X_3$-receptors present in neurones of the rat dorsal root ganglia. *Br J Pharmacol* **124:**176–180.
Rettinger J, Braun K, Hochmann H, Kassack MU, Ullmann H, Nickel P, Schmalzing G, and Lambrecht G (2005) Profiling at recombinant homomeric and heteromeric rat P2X receptors identifies the suramin analogue NF449 as a highly potent $P2X_1$ receptor antagonist. *Neuropharmacology* **48:**461–468.
Rettinger J and Schmalzing G (2004) Desensitization masks nanomolar potency of ATP at the $P2X_1$ receptor. *J Biol Chem* **279:**6426–6433.
Rettinger J, Schmalzing G, Damer S, Müller G, Nickel P, and Lambrecht G (2000) The suramin analogue NF279 is a novel and potent antagonist selective for the $P2X_1$ receptor. *Neuropharmacology* **39:**2044–2053.
Souslova V, Cesare P, Ding Y, Akopian AN, Stanfa L, Suzuki R, Carpenter K, Dickenson A, Boyce S, Hill R, et al. (2000) Warm-coding deficits and aberrant inflammatory pain in mice lacking $P2X_3$ receptors. *Nature (Lond)* **407:**1015–1017.
Ullmann H, Meis S, Hongwiset D, Marzian C, Wiese M, Nickel P, Communi D, Boeynaems JM, Wolf C, Hausmann R, et al. (2005) Synthesis and structure-activity relationships of suramin-derived $P2Y_{11}$ receptor antagonists with nanomolar potency. *J Med Chem* **48:**7040–7048.
Virginio C, Robertson G, Surprenant A, and North RA (1998) Trinitrophenyl-substituted nucleotides are potent antagonists selective for $P2X_1$, $P2X_3$ and heteromeric $P2X_{2/3}$ receptors. *Mol Pharmacol* **53:**969–973.
Werner P, Seward EP, Buell GN, and North RA (1996) Domains of P2X receptors involved in desensitization. *Proc Natl Acad Sci USA* **93:**15485–15490.

Address correspondence to: Dr. Günther Schmalzing, Department of Molecular Pharmacology, University Hospital of RWTH Aachen University, Wendlingweg 2, 52074 Aachen, Germany. E-mail: gschmalzing@ukaachen.de